Measurement and analysis of the surface roughness of Ag film used in plasmonic lithography*

Gao-Feng Liang(梁高峰)[1,2], Jiao Jiao(焦蛟)[1], Xian-Gang Luo(罗先刚)[2], and Qing Zhao(赵青)[1,†]

[1] School of Physical Electronics, University of Electronic Science and Technology of China, Chengdu 610054, China
[2] State Key Laboratory of Optical Technologies for Microfabrication, Institute of Optics and Electronics, Chinese Academy of Sciences, Chengdu 610209, China

(Received 3 August 2016; revised manuscript received 30 September 2016; published online 29 November 2016)

The silver (Ag)/photoresist (PR)/Ag structure, widely used in plasmonic photolithography, is fabricated on silicon substrate. The surface roughness of the top Ag film is measured and analyzed systematically. In particular, combined with template stripping technology, the lower side of the top Ag film is imaged by an atomic force microscope. The topographies show that the lower side surface is rougher than the initial surface of the subjacent PR film, which is mainly attributable to the deformation caused by particle collisions during the deposition of the Ag film. Additionally, further measurements show that the Ag film deposited on the PR exhibits a flatter upper side morphology than that directly deposited on the silicon substrate. This is explained by the different growth modes of Ag films on different substrates. This work will be beneficial to morphology analysis and performance evaluation for the films in optical and plasmonic devices.

Keywords: surface roughness, lithography, silver film, deposition

PACS: 68.35.Ct, 81.16.Nd, 68.55.–a, 81.15.–z **DOI:** 10.1088/1674-1056/26/1/016801

1. Introduction

Plasmonics enable the nanoscale manipulation of optical signals by coupling light to coherent electronic excitations at the interface between dielectric and metal materials.[1] The strong confinement of light associated with surface plasmon (SP) resonances has stimulated the development of nanophotonic components such as waveguides,[2] switches,[3] sensors,[4] and metamaterials.[5–7] In the above applications, the films must usually be very thin and flat to achieve efficient coupling between the light and SP. However, the surface roughness remains an important factor in the design of nano-optical devices.[8,9] For example, the silver (Ag)/photoresist (PR)/Ag structure is often used in nanolithography to realize sub-wavelength imaging beyond the diffraction limit.[10,11] The interface roughness between the top Ag film and the PR film is critical in achieving the desired goals.[11,12] Therefore, to effectively analyze the device performance, it is necessary to identify the precise surface morphology. However, in bottom-up stacked film systems, if the variations caused by subsequent film deposition are not considered,[13–15] using the surface roughness of the subjacent film as the interface roughness between the two films is unreliable.

Recently, template stripping (TS) technology has attracted a great deal of attention in the field of nanofabrication because of its special ability to reverse the structure and generate ultra-smooth surfaces.[16] Generally, the device structure is fabricated on a template substrate and attached to another substrate with curable epoxy adhesive that can be stripped off from the template substrate perfectly.[17] Thus, the bottom surface of the device can be measured directly in this reversed structure. The key requirement for TS is to generate an interface with weak adhesion between the template and structure. Usually, the silicon and several metals are used as the template substrate and structure materials,[18,19] where the metals can also be used in plasmonic devices.[20,21]

In this study, the Ag/PR/Ag structure is examined to demonstrate the effectiveness of the method in measuring the morphology of both sides of the top Ag film. Firstly, the upper side of the stacked film is measured by an atomic force microscope (AFM). Then, combined with TS technology, the lower side of the top Ag film is revealed. Measurements show that the lower side morphology of the top Ag film is rougher than the initial upper side morphology of the subjacent PR film. Additionally, the Ag films are measured on two different substrates. The surface roughness indicates that the Ag film on a thin PR film exhibits an improved upper side morphology, with a noticeably smaller root-mean-square (RMS) surface roughness and narrower peak-to-peak (P-P) surface topological distance distribution than that directly deposited on the silicon substrate.

*Project supported by the National Basic Research Program of China (Grant No. 2013CBA01702) and the National Natural Science Foundation of China (Grant No. 11275045).

†Corresponding author. E-mail: zhaoq@uestc.edu.cn

© 2017 Chinese Physical Society and IOP Publishing Ltd

2. Roughness measurement of both sides of an Ag film

The diagram in Fig. 1 shows an example of the stacked Ag/PR/Ag structure used in plasmonic lithography. Here, it is fabricated to show the measurement of the morphology of both sides of the top Ag film. The films are set to be Ag (20 nm)/PR (30 nm)/Ag (60 nm) from top to bottom, where the lower side surface of the top Ag film (20 nm) is regarded as the interface between the top Ag/PR.

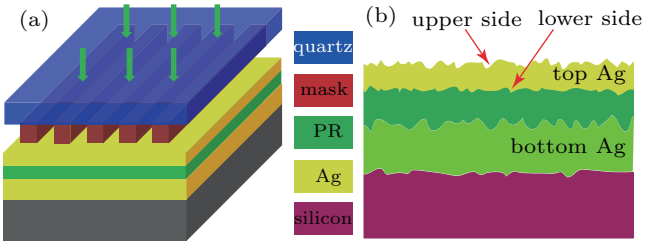


Fig. 1. (color online) (a) Diagram of the Ag/PR/Ag structure used in photolithography. (b) Cross section of the Ag/PR/Ag structure with rough surfaces.

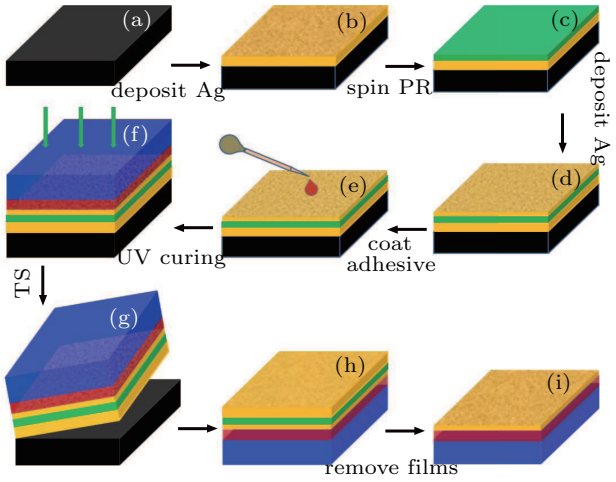


Fig. 2. (color online) Diagrams of the fabrication processes for measuring surface morphology.

The processes are shown in Fig. 2. To avoid exposing the PR during the deposition processes of sputtering or e-beam evaporation, all the Ag films were deposited by thermal evaporation at a base pressure of $\sim 5.0 \times 10^{-4}$ Pa and at the ambient temperature. Prior to the deposition, the silicon substrate was first boiled for 1 h at 393.15 K in a composite solution of H_2SO_4:H_2O_2 (3:1). The substrate was then cleaned ultrasonically in acetone and deionized water sequentially, and finally dried with nitrogen. This leaves a natural oxide layer ($\sim$ 1–3 nm thick) on the substrate, which is referred to as the SiO_2/Si(100) substrate. Because the surface roughness increases almost linearly with deposition rate,[22] the Ag films were deposited with a low and stable deposition rate (2 Å/s), as monitored by a quartz crystal oscillator. Subsequently, an AFM was used to measure the surface morphology. The surface roughness, in the RMS sense (R_q), and the P-P distance difference were determined via AFM topography values followed by a quantitative and statistical surface analysis. For a surface in the x-y plane, its roughness can be calculated as

$$R_q = \sqrt{\frac{1}{M}\frac{1}{N}\sum_{x=1}^{M}\sum_{y=1}^{N}(z(x,y)-\bar{z})^2}$$

where $\bar{z}$ is the average height of the topography as a reference of the x–y plane; z is the altitude difference relative to $\bar{z}$ at (x,y); M and N are the number of topography values along the x and y directions, respectively. The histogram of surface roughness offers a quantitative measure of the maximum P-P distance and the average surface height deviation.[23]

2.1. Upper side measurement

Firstly, the 60 nm-thick Ag film was deposited on SiO_2/Si(100) substrate (Fig. 2(b)). The upper side morphology is shown in Figs. 3(a) and 3(d). The surface roughness of this film, measured in a 5×5 μm^2 (256×256 pixels) scan area, is approximately 1.2 nm in the RMS sense with a maximum P-P distance of about 9.04 nm. Secondly, the diluted AR-3170 positive PR was spun onto the Ag film (Fig. 2(c)). After being baked at 373.15 K for 5 min on a hotplate, the PR film had a thickness of about 30 nm, as measured with a surface profiler. Its upper side morphology was very flat due to the reflow effect, as shown in Figs. 3(b) and 3(e). The RMS roughness was $\sim$ 0.32 nm and the maximum P-P distance was $\sim$ 2.67 nm. Subsequently, the 20 nm-thick Ag film was evaporated on PR as the top film (Fig. 2(d)). Its upper side morphology is shown in Figs. 3(c) and 3(f). The RMS roughness was $\sim$ 0.57 nm and the maximum P-P distance was $\sim$ 5.28 nm. This procedure completely fabricates the Ag/PR/Ag structure.

2.2. Lower side measurement

The Ag/PR/Ag structure was then separated from the SiO_2/Si(100) substrate by TS technology. First, another quartz substrate was glued onto the top Ag film with epoxy adhesive,[24] which is a type of polymer that can be solidified by UV light. This was illuminated by a filtered mercury lamp with a radiation peak at 365 nm from the side of the quartz. This adhesive layer can be completely cured with an exposure dosage of 100 J/cm^2. Consequently, the Ag/PR/Ag is surrounded by quartz and SiO_2/Si(100) substrates. Because of the weak adhesion between Ag and the SiO_2/Si(100) substrate, the Ag/PR/Ag together with the quartz substrate can be totally stripped off from the SiO_2/Si(100) substrate. Therefore, the quartz substrate changes into the support substrate, and the lower side surface of the 60 nm-thick Ag film becomes an exposed surface (Fig. 2(h)). Because the TS technology leads to a flat surface without any terraces or steps, the AFM images of this surface are an approximation of the template substrate, as shown in Figs. 4(a) and 4(c). The RMS roughness was $\sim$ 0.31 nm with a maximum P-P distance of $\sim$ 7.28 nm.

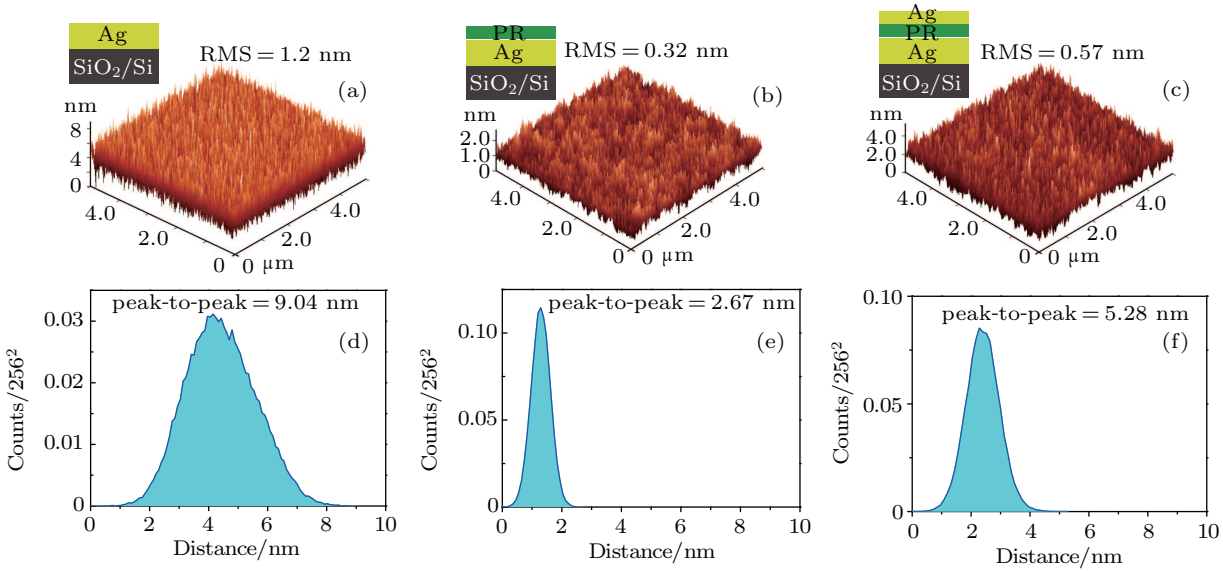


Fig. 3. (color online) Upper side morphology variations during Ag/PR/Ag fabrication correspond to the surfaces in Figs. 2(b)–2(d), respectively. The surface roughness measured by AFM over a 5×5 μm^2 area is (a) ∼ 1.2 nm for Ag/SiO_2/Si, (b) ∼ 0.32 nm for PR/Ag/SiO_2/Si, and (c) ∼ 0.57 nm for Ag/PR/Ag/SiO_2/Si, respectively. (d)–(f) Histograms of the surface height values from the respective topographies.

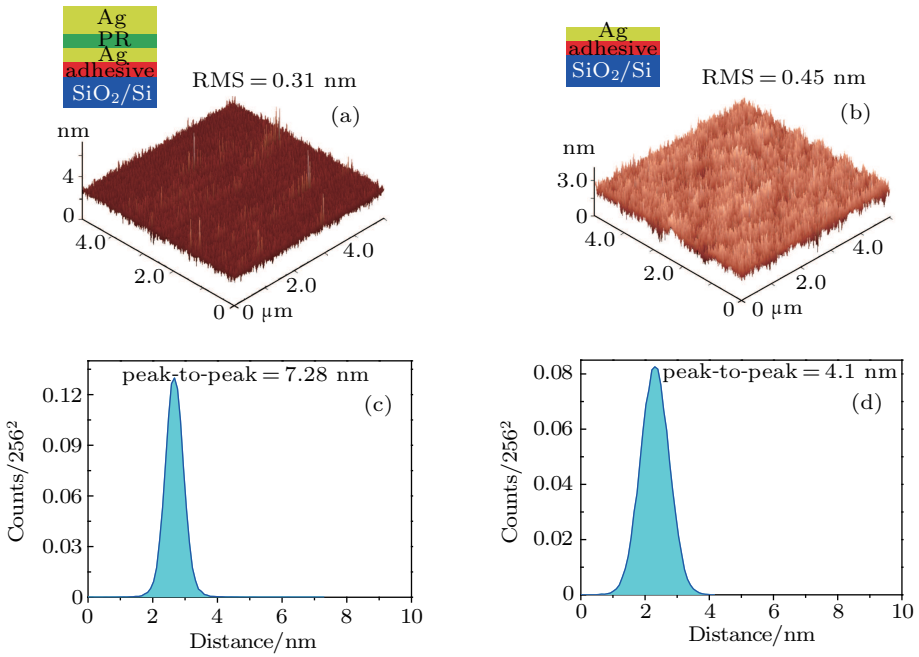


Fig. 4. (color online) Lower side morphology variations during TS correspond to the surfaces in Figs. 2(h) and 2(i), respectively. The surface roughness is (a) ∼ 0.31 nm for Ag/PR/Ag/Quartz and (b) ∼ 0.45 nm for Ag/Quartz, respectively. (c), (d) Histograms of the surface height values from the respective topographies.

The 60 nm-thick Ag film was cleaned with diluted chromium remover. The 20 nm-thick Ag film was not dissolved because of the 30 nm-thick PR shielding layer, which was subsequently cleaned by acetone solution. Finally, the desired lower side of the 20 nm-thick Ag film was exposed (Fig. 2(i)). The AFM images in Figs. 4(b) and 4(d) show that its RMS roughness is ∼ 0.45 nm and the maximum P-P distance is ∼ 4.1 nm, which is rougher than the initial PR surface (Figs. 2(c), 3(b), and 3(e)). This is caused by the damage to the upper side morphology of the PR film during the top Ag deposition. During the formation of the top Ag film, the Ag particles that evaporate in the vacuum cavity collide with the upper side of the PR film, and the kinetic energy of these particles would cause them to impact into the PR surface, leaving a protrusion after TS and the removal of the PR layer. This results in the rougher interface morphology of the top Ag/PR.

Superlens-based lithography achieves sub-wavelength resolutions using a thin slab of metal to amplify the transverse magnetic polarized evanescent waves.[10,11] However, this technique is very sensitive to the quality of the film. The edge and surface roughness of the film will cause localized SP resonance, leading to a nonuniform intensity field distribution. A two-dimensional (2D) electric field intensity distribution imaged from the 90 nm period grating mask is shown

in Fig. 5. When P-polarized light with 365 nm wavelength illuminates the lithography structure with smooth films (RMS = 0 nm) from the top side, the intensity distribution is uniform. The profile, taken from the middle position of the PR film, presents a pattern with high intensity contrast. However, when the roughness is introduced to the surfaces of the stacked films, the field distribution is severely distorted. The surface roughness of the Ag/PR/Ag structure in Fig. 5(b) is 0.57 nm/0.32 nm/1.2 nm from top to bottom. As a comparison, figure 5(c) shows rough films with RMS roughness of 0.57 nm/0.45 nm/1.2 nm at the corresponding surfaces. It can be clearly seen that the pattern in Fig. 5(f) presents weaker intensity and lower contrast than that in Fig. 5(e). This shows that the performance of superlens-based lithography is deeply related to the quality of the films. However, the morphology variation during deposition makes the interface roughness between the top Ag/PR (0.45 nm) somewhat different from the initial surface roughness of the PR film (0.32 nm). Thus, it is not accurate to consider the initial surface morphology of the PR film as the interface morphology of the top Ag/PR.

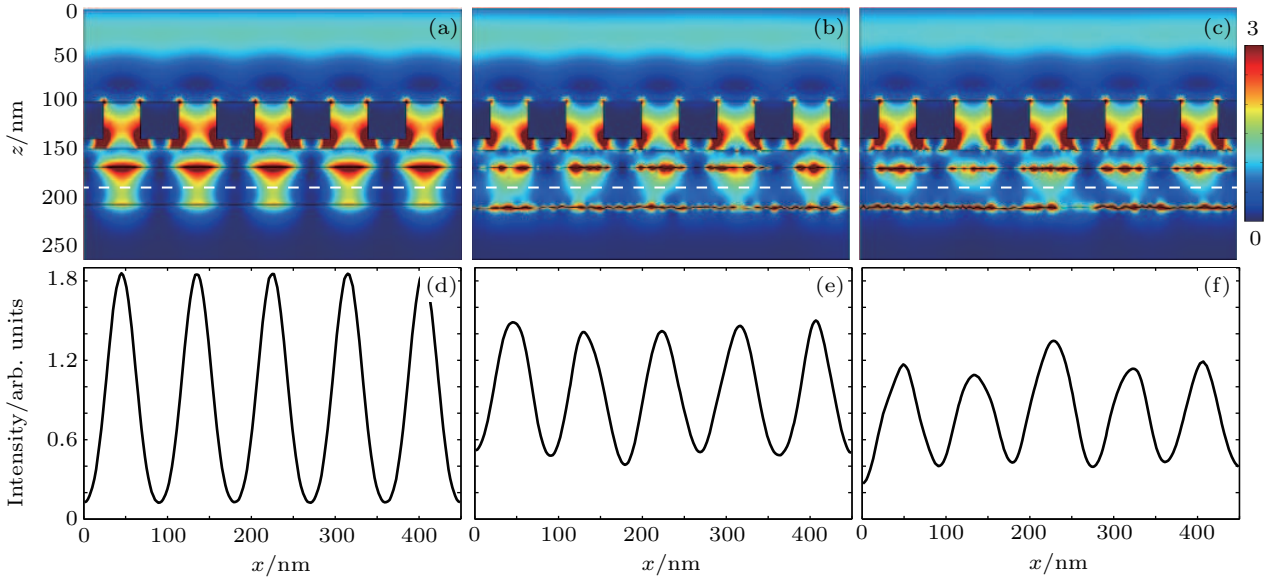


Fig. 5. (color online) Normalized electric field intensity distribution of 90 nm period grating mask imaged in the PR film. (a) All the surface roughnessnesses of the Ag/PR/Ag structure are 0 nm. (b) The surface roughnesses of the Ag/PR/Ag structure are 0.57 nm/0.32 nm/1.2 nm from top to bottom. (c) The surface roughnesses of the Ag/PR/Ag structure are 0.57 nm/0.45 nm/1.2 nm from top to bottom. (d)–(f) Intensity profiles at the dashed line positions in (a)–(c), respectively.

3. Morphology comparison of films on different substrates

Comparing the results in Figs. 3(a) and 3(c), the upper side morphology of the top 20 nm-thick Ag film is much flatter than that of the 60 nm-thick Ag film, which may be related to the thickness of the film and the flatness of the substrate. Additionally, the substrate material is an important factor for the deposition of flat films, which is demonstrated here by the surface roughness of 100 nm-thick Ag films deposited on two different substrate materials. The AFM topography in Figs. 6(a) and 6(c) shows the upper side of an Ag film deposited on the SiO_2/Si(100) substrate. Its surface roughness is $\sim$ 1.63 nm with a maximum P-P distance of $\sim$ 11.28 nm. In the comparative experiment, the diluted AR-3170 positive PR was first spun onto the SiO_2/Si(100) substrate and baked at 373.15 K for 5 min on a hotplate. After that, the 100 nm-thick Ag film was deposited onto this PR/SiO_2/Si(100) substrate; the upper side morphology of this substrate is shown in Figs. 6(b) and 6(d). Its surface roughness is $\sim$ 0.75 nm with a maximum P-P distance of $\sim$ 8.94 nm. Note that the roughness of the PR film shown in Fig. 3(b) is 0.32 nm, and the SiO_2/Si(100) substrate is the template for the lower side of the 60 nm-thick Ag film, which has a roughness of 0.31 nm, as shown in Fig. 4(a). Therefore, it can be concluded that Ag film deposited on PR film is much flatter than that on the SiO_2/Si(100) substrate, even though the initial upper side of the PR film may be a little rougher than the polished SiO_2/Si(100) substrate.

Based on further measurements, figure 7 shows a clear relationship between the surface roughness and Ag thickness corresponding to SiO_2/Si(100) and PR/SiO_2/Si(100) substrates, where the curves indicate the possible changing trend of roughness with different thickness of Ag films. As the thickness of the Ag film increases from 20 to 160 nm, the RMS values increase continuously for both substrates. The average surface roughness of the Ag film deposited on SiO_2/Si(100) substrate, i.e., the Ag/SiO_2/Si(100) sample denoted by black squares, increases from 1.01 to 2.36 nm, whereas that of the Ag film deposited on PR/SiO_2/Si(100) substrate, i.e., the Ag/PR/SiO_2/Si(100) sample denoted by red dots, increases from 0.5 to 1.63 nm. Therefore, the trends illustrate that

thicker Ag film leads to larger roughness in the RMS sense for both substrates. Moreover, note that all the RMS values of the Ag/PR/SiO_2/Si(100) sample are smaller than those of the Ag/SiO_2/Si(100) sample for Ag films with the same thickness conditions. This indicates that Ag film on the PR/SiO_2/Si(100) substrate has a flatter upper side morphology than that on the SiO_2/Si(100) substrate. Hence, the substrate material is also a critical factor for the flatness of film deposition.

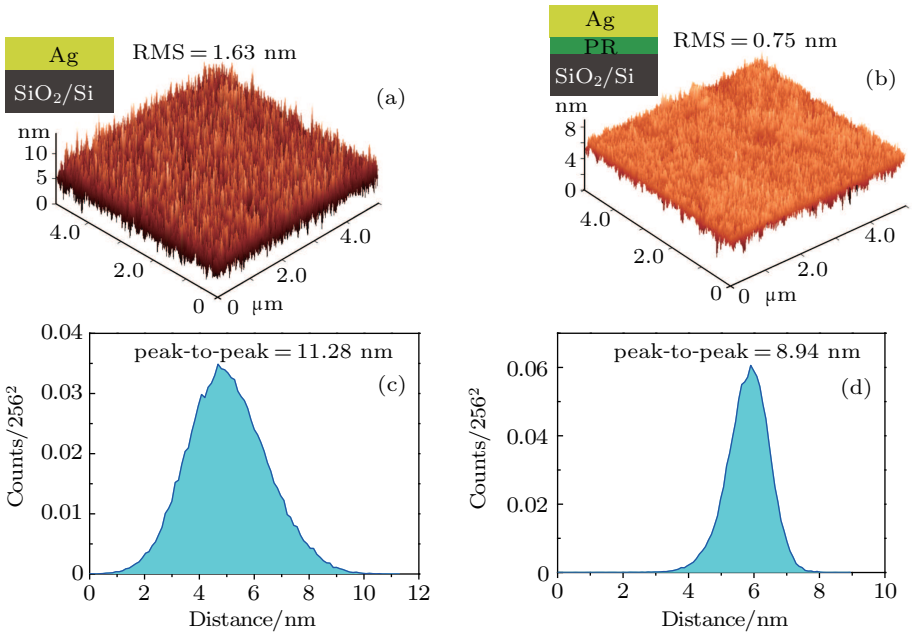


Fig. 6. (color online) Upper side morphologies represented by AFM images over an area of 5×5 μm^2 (256×256 pixels): (a) 100 nm-thick Ag film on SiO_2/Si(100), (b) 100 nm-thick Ag film on PR/SiO_2/Si(100). (c), (d) Histograms of the surface height values from the respective topographies.

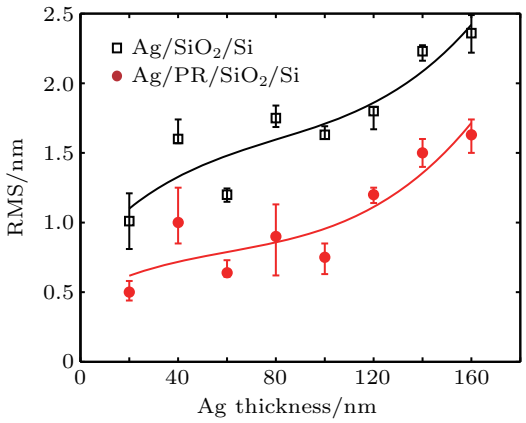


Fig. 7. (color online) The relationship between surface roughness and thickness of Ag films corresponding to SiO_2/Si(100) and PR/SiO_2/Si(100) substrates. The RMS values of Ag/SiO_2/Si(100) samples and Ag/PR/SiO_2/Si(100) samples are denoted by squares and dots with error bars, respectively. Both solid curves represent the possible changing trends of the RMS values.

This phenomenon can be explained by the deposition models of particles. At the beginning of the film formation, the growth of thin film depends significantly on the interaction strength between the deposited atoms and the substrate, resulting in three different growth modes.[25,26] For the Volmer–Weber, or island growth mode (Fig. 8(a)), atom–atom interactions are stronger than those between atoms and the substrate. The atoms that fall onto the substrate diffuse and migrate on the surface. Neighboring atoms coagulate into clusters or islands, which then further combine together to form a film on the substrate surface.[27] However, pinholes are formed when the islands coalesce to film, leading to a relatively rough surface. The Ag film growth on SiO_2/Si(100) substrate is likely to occur via this mode.[28] Figure 8(d) is a scanning electron microscopy (SEM) image of Ag film of thickness 20 nm on the SiO_2/Si(100) substrate. For the Frank–van der Merwe, or layer-by-layer growth mode (Fig. 8(b)), the atom–atom interactions are weaker than those between atoms and substrate. Atoms attach preferentially to surface sites resulting in an atomically flat and fully formed film. The final intermediate case is Stranski–Krastanov, or layer–island growth mode (Fig. 8(c)). In this case, the layer formation is completed before island growth begins at a critical layer thickness.[29] The Ag film growth with PR/SiO_2/Si(100) substrate is most likely via this mode, with the thin PR layer working as a kind of wetting material.[28–30] During the deposition of the first several layers, the Ag atoms, which may only diffuse a few tens of nanometers, are adsorbed directly on the PR surface. The growth mode of Ag film then switches to island growth mode. Hence, as the Ag film thickness increases in Fig. 7, the RMS values of the Ag/PR/SiO_2/Si(100) sample initially increase at a slower rate than those of the Ag/SiO_2/Si(100) sample, then subsequently rise at a comparable rate. However, layer–island growth mode can still form a more continuous Ag film with a flatter surface and a higher grain boundary density,[30,31] as

shown by the SEM image in Fig. 8(e). Thus, the morphologies would be very different for films deposited on different materials. It is not rigorous to consider the same surface morphology for films on different substrates, even though they may be deposited using the same parameters.

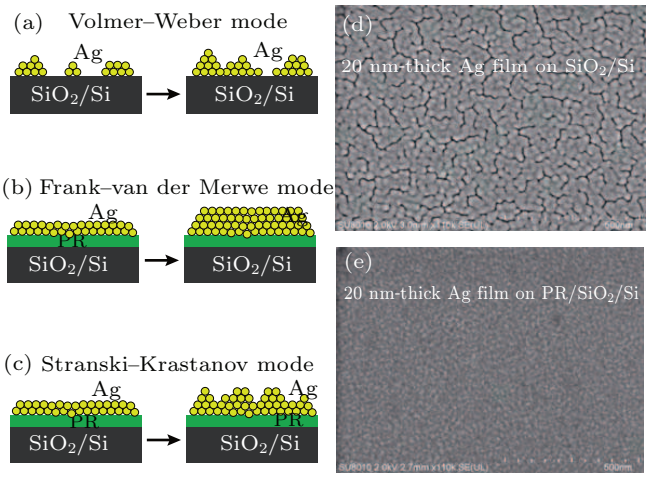


Fig. 8. (color online) Diagrams of Ag film growth in (a) Volmer–Weber mode, (b) Frank–van der Merwe mode, and (c) Stranski–Krastanov mode. SEM images of 20 nm thick Ag film on (d) SiO_2/Si(100) substrate and (e) PR/SiO_2/Si(100) substrate, respectively.

4. Conclusion

In this study, the morphology of both sides of the top Ag film in an Ag/PR/Ag structure has been measured and analyzed, and the results illustrated using AFM and SEM images. We have found that the lower side morphology of the top Ag film is a little rougher than the initial upper side morphology of the subjacent PR film. This can be attributed to the particle collisions that occur during the deposition of the top Ag film causing some morphology variation in the PR film. In addition, the wetting effect of the PR film causes the Ag film to grow in layer–island mode, meaning that the upper side morphology of an Ag film deposited on a PR film exhibits smaller surface roughness than that of an Ag film deposited directly on a SiO_2/Si(100) substrate. This paper has investigated and described the surface morphology of stacked films. Our results will be beneficial to morphological analysis and performance evaluation of films in optical and plasmonic devices.

Acknowledgment

We thank Z Guo and Z Zhao for kind help on experiment, and thank Prof. C Wang for helpful discussion.

References

[1] Barnes W L, Dereux A and Ebbesen T W 2003 *Nature* **424** 824
[2] Chen J, Smolyakov G A Brueck S R J and Malloy K J 2008 *Opt. Express* **16** 14902
[3] Liu Y J, Zheng Y B Liou J, Chiang I, Khoo I C and Huang T J 2011 *J. Phys. Chem. C* **115** 7717
[4] Zhang X P, Ma X M, Dou F, Zhao P X and Liu H M 2011 *Adv. Funct. Mater.* **21** 4219
[5] Liang G F, Wang C T, Zhao Z Y, Wang Y Q, Yao N, Gao P, Luo Y F, Gao G H, Zhao Q and Luo X G 2015 *Adv. Opt Mater.* **3** 1248
[6] Liang G F, Zhao Z Y, Yao N, Wang C T, Jiang B, Zhao Q and Luo X G 2014 *J. Nanophotonics* **8** 083080
[7] Liang G F, Zhao Q, Chen X, Wang C T, Zhao Z Y and Luo X G 2012 *Acta Phys. Sin.* **61** 104203 (in Chinese)
[8] Ma X Z, Zhang R, Sun J B, Shi Y and Zhao Y 2015 *Chin. Phys. Lett.* **32** 045202
[9] Luo Z Y, Tang J, Ma B, Zhang Z Z, Jin Q Y and Wang J P 2012 *Chin. Phys. Lett.* **29** 127501
[10] Xu F Y, Chen G H, Wang C H, Cao B and Lou Y M 2013 *Opt. Lett.* **38** 3819
[11] Gao P, Yao N, Wang C T, Zhao Z Y, Luo Y F, Wang Y Q, Gao G H, Liu K P, Zhao C W and Luo X G 2015 *Appl. Phys. Lett.* **106** 093110
[12] Guo Z, Huang Q Z, Wang C T, Gao P, Zhang W, Zhao Z Y, Yan L S and Luo X G 2014 *Plasmonics* **9** 103
[13] Xue B Q, Chang H D, Sun B, Wang S K and Liu H G 2012 *Chin. Phys. Lett.* **29** 046801
[14] Zhou X, Luo Z J, Wang J H, Guo X and Ding Z 2015 *Acta Phys. Sin.* **64** 216803 (in Chinese)
[15] Duan F L, Wang M and Liu J 2015 *Acta Phys. Sin.* **64** 066801 (in Chinese)
[16] Vogel N, Zieleniecki J and Köper I 2012 *Nanoscale* **4** 3820
[17] Nagpal P, Lindquist N C, Oh S H and Norris D J 2009 *Science* **325** 594
[18] Wagner P, Hegner M, Guntherodt H J and Semenza G 1995 *Langmuir* **11** 3867
[19] Weiss E A, Kaufman G K, Kriebel J K, Li Z, Schalek R and Whitesides G M 2007 *Langmuir* **23** 9686
[20] Jiao J, Zhao Q, Li X, Liang G F, Huang X P and Luo X G 2014 *Opt. Express* **20** 26277
[21] Hecht B, Bielefeldt H, Novotny L, Inouye Y and Pohl D W 1996 *Phys. Rev. Lett.* **77** 1889
[22] Leong E S, Liu Y J, Wang B and Teng J 2011 *ACS Appl. Mater. Inter.* **3** 1148
[23] Higo M, Fujita K, Tanaka Y, Mitsushio M and Yoshidome T 2006 *Appl. Surf. Sci.* **252** 5083
[24] X31213, Zymet Inc., www. Zymet.com, E. Hanover, NJ 07936, USA
[25] Venables J A 2000 *Introduction to Surface and Thin Film Processes* (Cambridge: Cambridge University Press) p. 145
[26] Oura K, Lifshits V G, Saranin A A, Zotov A V and Katayama M 2003 *Surface Science: An Introduction* 1st edn. (Berlin: Springer) p. 357
[27] McBrayer J D, Swanson R M and Sigmon T W 1986 *J. Electrochem. Soc.* **133** 1242
[28] Logeeswaran V J, Kobayashi N P, Islam M S, Wu W, Chaturvedi P, Fang N X, Wang S Y and Williams R S 2009 *Nano Lett.* **9** 178
[29] People R and Bean J C 1985 *Appl. Phys. Lett.* **47** 322
[30] Ke L, Lai S C, Liu H, Peh C K N, Wang B and Teng J H 2012 *ACS Appl. Mater. Inter* **4** 1247
[31] Chen W Q, Thoreson M D, Ishii S, Kildishev A V and Shalaev V M 2010 *Opt. Express* **18** 5124